Temperature cycling and its effect on mechanical behaviours of high-porosity chalks

Voake, T.; Nermoen, A.; Korsnes, R. I.; Fabricius, I. L.

Published in:
Journal of Rock Mechanics and Geotechnical Engineering

Link to article, DOI:
10.1016/j.jrmge.2018.11.010

Publication date:
2019

Document Version
Publisher's PDF, also known as Version of record

Journal of Rock Mechanics and Geotechnical Engineering 11 (2019) 749–759

Contents lists available at ScienceDirect

Journal of Rock Mechanics and Geotechnical Engineering

journal homepage: www.rockgeotech.org

Full Length Article

Temperature cycling and its effect on mechanical behaviours of high-porosity chalks

T. Voake [a,b,*], A. Nermoen [b,c], R.I. Korsnes [a,b], I.L. Fabricius [a,d]

[a] University of Stavanger, Stavanger, Norway
[b] The National IOR Centre of Norway, University of Stavanger, Stavanger, Norway
[c] International Research Institute of Stavanger (IRIS), Stavanger, Norway
[d] Technical University of Denmark (DTU), Copenhagen, Denmark

ARTICLE INFO

Article history:
Received 23 July 2018
Received in revised form
8 October 2018
Accepted 26 November 2018
Available online 23 April 2019

Keywords:
Elastoplastic partitioning
Anisotropic thermal expansion
Strain accumulation due to temperature and stress cycles

ABSTRACT

Temperature history can have a significant effect on the strength of water-saturated chalk. In this study, hydrostatic stress cycles are applied to understand the mechanical response of chalk samples exposed to temperature cycling between each stress cycle, compared to the samples tested at a constant temperature. The total accumulated strain during a stress cycle and the irreversible strain are reported. Chalk samples from Kansas (USA) and Mons (Belgium), with different degrees of induration (i.e. amount of contact cementation), were used. The samples were saturated with equilibrated water (polar) and non-polar Isopar H oil to quantify water weakening. All samples tested during 10 stress cycles with varying temperature (i.e. temperature cycled in between each stress cycle) accumulated more strain than those tested at constant temperatures. All the stress cycles were performed at 30 °C. The two chalk types behaved similarly when saturated with Isopar H oil, but differently when saturated with water. When saturated with water, the stronger Kansas chalk accumulated more total strain and more irreversible strain within each stress cycle than the weaker Mons chalk.

1. Introduction

Intermittent cold-water injection into a warm reservoir during oil production, or injection of supercritical CO_2 for carbon storage, would lead to cooling that could thermally degrade the formation surrounding an injection well. Thermal strain may potentially cause permanent damage, especially to a rock composed of anisotropic minerals, and eventually lead to well instability. This paper focuses on chalk reservoirs, where the proposed effect could be of high relevance, because chalk is primarily composed of calcite with a highly anisotropic thermal expansion coefficient. The calcite crystal has a trigonal axis of symmetry, with thermal expansion coefficients of $23.8 \times 10^{-6}\ K^{-1}$ and $-5.2 \times 10^{-6}\ K^{-1}$ in the directions parallel and perpendicular to the trigonal axis, respectively (Rosenholtz and Smith, 1949), thereby leading to thermal expansion and contraction when heated. For two calcite crystals in close contact with each other, with unaligned trigonal axis, a temperature increase leads to strain differences in the two crystals, which localises stress at the cemented particle contact. The premise of this paper is to investigate to what extent thermal variation leads to measurable mechanical degradation for centimetre scale cylindrical core samples.

Chalk is a carbonate rock whose particles originate from skeletons of phytoplanktonic coccolithophores (algae), forming calcareous ooze composed of calcite. As the calcareous ooze is buried deeper, the stress at particle contacts builds up, resulting in pressure dissolution and thus the formation of contact cement. More cemented deeper chalks possess a lower Biot coefficient and higher initial strength and stiffness than less cemented chalks with higher Biot coefficients (Fabricius, 2014).

In materials composed of anisotropic particles held together by inter-granular contact cement, the contact zones can localise significant stresses because of local differences in the thermal strain, even though the temperature in the sample is uniform. For example, marble which is mineralogically similar to chalk with calcite as its main constituent is known to degrade when exposed to outdoor temperature variation, and some marble facades consequently tend to experience concave bowing (Weiss et al.,

* Corresponding author.
E-mail address: tijana.voake@uis.no (T. Voake).
Peer review under responsibility of Institute of Rock and Soil Mechanics, Chinese Academy of Sciences.

https://doi.org/10.1016/j.jrmge.2018.11.010

2003). Hansen et al. (2003) found that marble cladding weakens with the number of years it has been exposed to seasonal climate, and that marble tested in the laboratory at 100% relative humidity accordingly weakens with increasing number of cooling and heating cycles; by contrast, dry samples tested did not demonstrate weakening upon temperature cycling. Similarly, no damage to a dry limestone was observed when it was heated up to 300 °C (Chen et al., 2009). Conversely, when tested for potential high-temperature thermal energy storage (≥573 °C), mafic and felsic rocks performed much better than limestone and sandstone, as thermal cycling leads to increases in porosity and mineral dehydration (Becattini et al., 2017). Tests on well casing cement indicated that thermal cycling caused cracking failure mechanism due to a decrease in tensile strength (De Andrade et al., 2015). Weathering induced thermal cycling also had an effect on a granitic dome in California, USA, where accumulation of thermal stress between layers induced subcritical cracking and triggered exfoliation (Collins et al., 2018).

Further, the impact of water moisture has been shown to play an important role in rock mechanics. Studies performed on fibreglass that underwent 500 thermal cycles from −40 °C to 25 °C indicated that the damage development was minimal for samples tested in a dry state, but much more pronounced in water-saturated samples (Okeson et al., 2006). Also, the tensile strength of sandstone has been demonstrated to be weakened by cyclically submerging samples in water for 48 h and drying them at 105 °C for 24 h. Half of the strength was lost after just seven repeated wetting and drying cycles (Hua et al., 2015). These studies show that temperature cycling has a more pronounced weakening effect in the presence of moisture.

Saturation with a polar pore fluid generally reduces the strength of porous rocks, as observed in sandstone (Baud et al., 2000; Wasantha and Ranjith, 2014), limestone (Lebedev et al., 2014), and chalk (Risnes et al., 2005). Wasantha and Ranjith (2014) analysed water-weakening of Hawkesbury sandstone (Australia) in the brittle regime and found that water saturation led to a 13%–38% reduction of initial dry strength, with higher decreases at higher confining pressures. Baud et al. (2000) used four different sandstones (Gosford, Berea, Boise, and Darley Dale) in their study. Their testing results showed brittle strength reduction of 5%–17%, where Gosford sandstone with the lowest porosity had the highest reduction and Berea sandstone with higher porosity was the least influenced by water saturation. They also reported that samples with higher fractions of altered feldspar and clay had more pronounced weakening by water saturation. Water weakening effects were also observed in argillaceous siltstone by a reduction in compressive and shear strengths (Yang et al., 2016).

Water weakening of chalks has gained much attention and many studies have been conducted focusing on chalk weakening mechanisms (e.g. Hermansen et al., 1997). Madland et al. (2002) found reductions in tensile strength and hydrostatic yield stress due to water saturation. Risnes et al. (2005) experimentally reported chalk strength as a function of water activity by mixing water and glycol as pore fluid, and a positive correlation was proposed. It has also been observed that the weakening effect is sensitive to fluid composition (Katika et al., 2015). Lisabeth and Zhu (2015) concluded that greater weakening in carbonate rocks is observed when pore fluid is far from equilibrium with the host rock, and also at higher temperatures. Similarly, Megawati et al. (2013) suggested that the weakening is enhanced with increasing negative surface charge of chalk due to pore fluid composition, where pore walls with greater negative charge would lead to greater overlap of electrical double layers and hence a rise in disjoining pressure.

In this paper, we explored how the mechanical hydrostatic stress cycles combined with temperature cycles affected the accumulation of strain in chalk. The effect of pore fluid was tested using two saturating solvents of different reactivities: water equilibrated with calcite and Isopar H oil. Also two chalk types from two different localities were selected, due to their differences in induration, Biot coefficient and associated amount of contact cementation between particles.

2. Materials and method

2.1. Materials

Chalks sampled from two quarries were used in this study, i.e. Kansas chalk from the Niobrara Formation, Fort Hays Member, USA (Late Cretaceous), and Mons chalk from the Trivières Formation, Harmignies, Belgium (Late Cretaceous). The two chalk blocks were selected because of their different degrees of induration, and hence different degrees of contact cementation. Induration is used for classification of carbonate rocks, with a four-point scale, H1 being loose and soft, and H4 being very strong and weakly metamorphosed. Kansas chalk has a larger contact area between the grains, which is reflected in its higher induration of H3 (Henriksen et al., 1999). The Mons chalk has a smaller contact area between the grains, which gives a lower induration of H2 (see Fig. 1). The Mons chalk has a carbonate content of 99.8% and a Biot coefficient, α, of 0.95, while the Kansas chalk has a carbonate content of 96.9% and a Biot coefficient of 0.91 (Ravnås, 2017).

From each chalk block, cylindrical cores of approximately 40 mm in diameter and 200 mm in length were drilled. The core diameter was adjusted to 38.1 mm, and each core was cut into plugs of about 70 mm in length. Eight plug samples from each block were prepared for testing (Table 1). The porosity was measured by using two methods. In the first method, porosity from saturation was calculated using the difference between dry and wet weights obtained by saturating the samples with distilled water in a vacuum

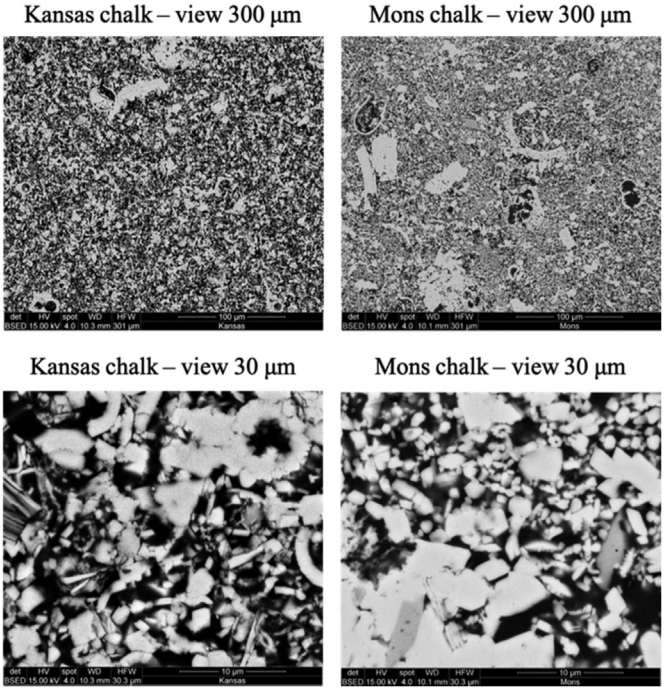

Fig. 1. Backscatter electron micrographs of Kansas and Mons chalks with two magnifications (30 μm and 300 μm images).

Table 1
Physical properties of samples used in this study. All samples had a diameter of 38.1 mm. Water is equilibrated with calcite.

Sample	Locality	Pore fluid	Temperature type	Length (mm)	ϕ_{sat} (%)	$\phi_{\rho_{gr}}$ (%)	V_p (m/s)
K19a	Kansas	Water	Cycled	72.1	35.4	35.5	
K40	Kansas	Water	Cycled	69.8	34.9	34.8	2860
K17a	Kansas	Water	Constant	73.5	35.1	35.3	
K18b	Kansas	Water	Constant	70.5	32.1	32	
K44a	Kansas	Isopar H oil	Cycled	70	34.6	34.8	2943
K22	Kansas	Isopar H oil	Cycled	73	33.9	34	3033
K25	Kansas	Isopar H oil	Constant	71.4	33	33.3	3043
K44b	Kansas	Isopar H oil	Constant	70	32.3	32.5	2942
M36b	Mons	Water	Cycled	70.4	43.8	44	2304
M31b	Mons	Water	Cycled	70	43.7	43.8	2288
M13	Mons	Water	Constant	68.8	44.4	42.9	2263
M24	Mons	Water	Constant	72.6	44.3	44.2	2298
M30	Mons	Isopar H oil	Cycled	70.2	42.6	42.6	2228
M36a	Mons	Isopar H oil	Cycled	67.8	41.5	41.7	2379
M18	Mons	Isopar H oil	Constant	71.8	43.1	43.4	2310
M32b	Mons	Isopar H oil	Constant	67	41.8	42.2	2335

Note: ϕ_{sat} and $\phi_{\rho_{gr}}$ are the porosity from saturation and porosity from grain density, respectively.

chamber. In the second method, porosity from grain density was derived from dry weight and volume of the samples, using the grain density of calcite (2.71 g/cm^3). P-wave velocity, V_p, was measured in dry state prior to saturating the samples with the pore fluid, using CNS Farnell PUNDIT 7 (precision ±0.1 μs). Based on these data and dry density, ρ_d, elastic P-wave modulus, M_p, was calculated as

$$M_p = \rho_d V_p^2 \quad (1)$$

Sixteen cylindrical core samples were tested, eight from each chalk type, of which four were saturated with calcite-equilibrated water of 0.652 mmol/L (polar fluid), and four with Isopar H oil (non-polar fluid). The equilibrated water was made by dissolving chalk powder in distilled water. Once the equilibrium was reached, the solution was filtered using a 0.65 μm filter. Both fluids were selected to minimise the impact of chemical reactions, thereby focussing this study on the rock–fluid interactions that are related to ion adsorption on mineral surfaces rather than dissolution and precipitation. Two of the four cores (with a given fluid and chalk type) were mechanically tested with constant temperature of 30 °C, and two were tested with a temperature cycle from 30 °C to 130 °C to 30 °C between each stress cycle. All stress cycles were performed at 30 °C. Each chalk type, fluid saturation, and temperature history were tested twice to investigate the repeatability of the results (see Table 1).

2.2. Mechanical tests

Mechanical tests on the samples were performed in a triaxial cell (see Fig. 2). Two different pumps were connected to the cell. The flow of the pore fluid was delivered by a Gilson pump (model 307 HPLC) while the confining pressure was controlled by a hydraulic Quizix pump, model QX-20000 HC. The confining pressure pump was equipped with two cylinders, assuring constant pressure applied. The pumps were individually operated through a LabVIEW routine. A back-pressure regulator was connected on the outlet side of the sample to ensure constant pore pressure of 0.7 MPa. The cell was also equipped with a 1000 W heating jacket controlled by an Omron E5CN PID temperature controller. The precision of the temperature controller is ±0.1 °C. The vertical displacement of the sample was measured by linear variable displacement transducer (LVDT, MHR 250 from Measurement Specialties™). The radial deformation was measured using an extensometer, where the circumference changes were detected by LVDT MHR 100 from Measurement Specialties™.

Volumetric strain was measured from the relative changes in length and diameter compared to the original dimensions of the

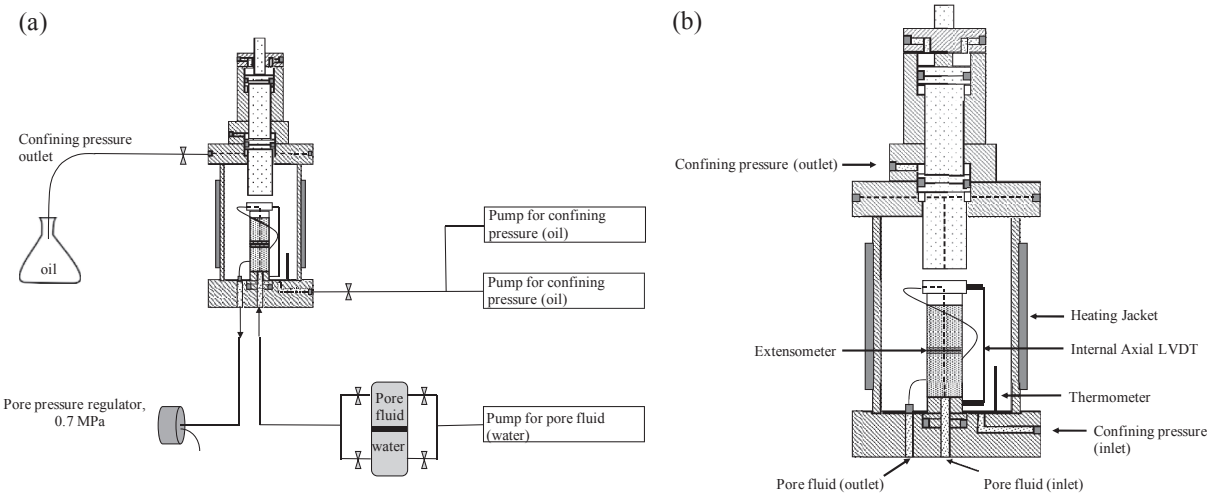

Fig. 2. (a) Experimental setup, and (b) triaxial cell with pressure regulating system.

cylindrical samples. Here, the volumetric strain of the cylindrical sample was estimated (omitting higher order terms) by

$$\varepsilon_{\mathrm{vol}} = \varepsilon_z + 2\varepsilon_{\mathrm{r}} \tag{2}$$

where ε_z is the axial strain from the change in length of the core, and ε_{r} is the radial strain measured by the change in the sample's diameter.

Hydrostatic stress cycles, i.e. the loading/unloading cycles, were performed by controlling the pressure in the hydraulic oil in the triaxial chamber, thus the applied pressure was equal at all sides, i.e. σ_{hyd}. The effective stress, σ_{eff}, experienced by the porous material was determined by

$$\sigma_{\mathrm{eff}} = \sigma_{\mathrm{hyd}} - \alpha P_{\mathrm{pore}} \tag{3}$$

where P_{pore} is the pore pressure. The effective hydrostatic stress changed from 0.5 MPa to 4.5 MPa over 30 min, and decreased back to 0.5 MPa over 30 min when the volumetric strain was measured (Fig. 3a).

2.3. Material response to hydrostatic stress cycling

The peak volumetric strain (Fig. 3a) at the maximal stress was divided into reversible $\varepsilon_{\mathrm{rev}}$ (elastic) and irreversible $\varepsilon_{\mathrm{irr}}$ (plastic) components obtained at the end of the stress cycle (Fig. 3b). An additive division in the elastic and plastic behaviours was used:

$$\varepsilon_{\mathrm{tot}} = \varepsilon_{\mathrm{rev}} + \varepsilon_{\mathrm{irr}} \tag{4}$$

It has been found that the bulk modulus K calculated from the unloading slope between the hydrostatic effective stress and volumetric strain provides a better match to the static modulus obtained from ultrasonic velocity measurements (Olsen et al., 2008). The lower K obtained from the loading curve is interpreted to be caused by the closure of unloading cracks formed when the sample was acquired from field, which causes additional artificial strain, especially during the first loading. This strain also causes unnecessary variability in the reported data and furthermore, it can be minimised by analysing the upper part of the unloading curve in which the nonlinear effects are less significant (Olsen et al., 2008). Therefore, we estimated the bulk modulus K from the stress–strain curves as follows when the effective stress varied from 4.5 MPa to 3.8 MPa:

$$K = \frac{\partial \sigma_{\mathrm{eff}}}{\partial \varepsilon_{\mathrm{vol}}} \tag{5}$$

For completeness purpose, the average slopes of the complete loading and unloading curves (between 0.5 MPa and 4.5 MPa) are also reported. Since the experiment was performed in drained conditions, the Biot coefficient using K can be estimated as

$$\alpha \approx 1 - K/K_{\mathrm{min}} \tag{6}$$

where K_{min} = 70.8 GPa is the average bulk modulus of calcite (Mavko et al., 1998).

The experiments were performed according to the following procedures:

(1) Once a sample was mounted on the triaxial cell, the confining stress was increased to 0.5 MPa.
(2) Simultaneous increases in confining stress and pore pressure were performed up to 1.2 MPa and 0.7 MPa, respectively.
(3) Temperature was set to 30 °C and the setup was left to rest until stable diameter readings were obtained.
(4) The hydrostatic stress was increased from 1.2 MPa to 5.2 MPa over 30 min, immediately followed by unloading to 1.2 MPa at the same stress rate (0.133 MPa/min). At the same time, the volumetric strain was measured continuously so that the loading/unloading slope was estimated as an average value during both phases, along with the elastic modulus which was measured during the initial unloading phase. During the stress cycle, the reversible and irreversible strain components were measured.
(5) For the samples exposed to temperature cycling, the temperature was increased to 130 °C over approximately 90 min after the hydrostatic loading/unloading cycle was completed. Then the setup was left to stabilise at 130 °C for approximately 360 min, before the Omron E5CN PID temperature controller was set to 30 °C and the triaxial cell cooled during approximately 450 min and then stabilised overnight, until another cycle was performed. For the samples tested at a constant temperature, the temperature cycle was omitted (Fig. 4). The same time interval between each stress cycle was used in all tests, and all stress cycles were performed at 30 °C.
(6) Steps 4 and 5 were repeated 10 times continuously over 10 d.
(7) For the samples exposed to temperature cycling, an additional 11th hydrostatic stress cycle was performed, without a

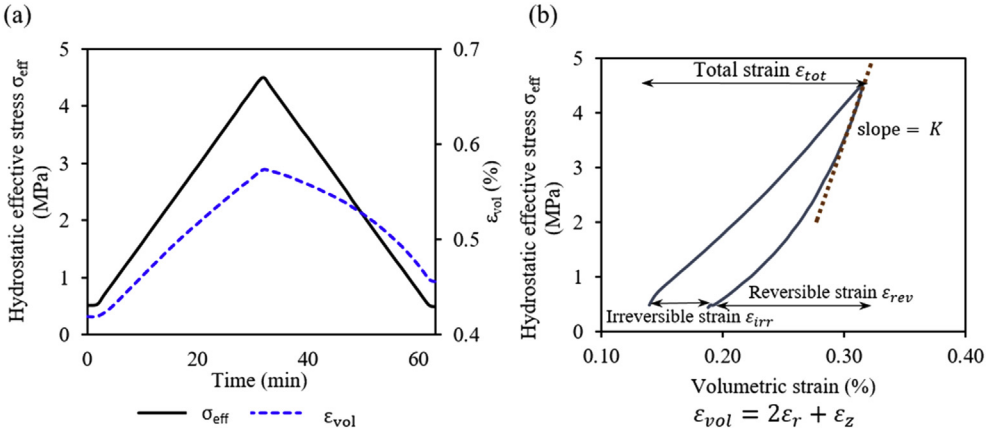

Fig. 3. Stress–strain relation during a stress cycle. (a) Strain response to stress changes. (b) After a complete stress cycle, strain is divided into elastic/reversible strain and plastic/irreversible strain. The elastic modulus K is measured as the slope of the steepest initial unloading phase.

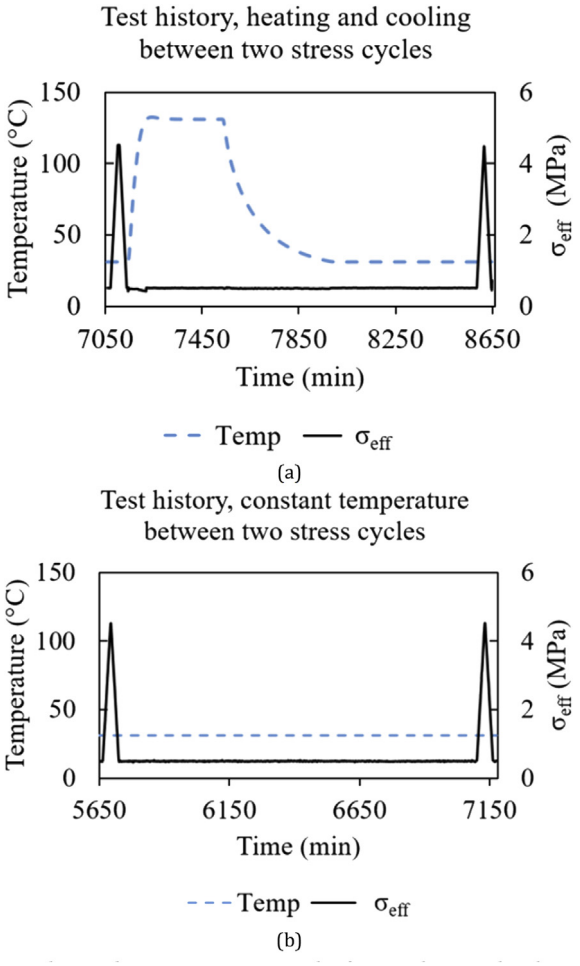

Fig. 4. (a) Test history between two stress cycles for samples tested with temperature cycling (in which a heat pulse is included between each stress cycle); and (b) Test history at constant temperature. The time interval between stress cycles were 24 h.

temperature cycle. This was to assess whether the observed stress–strain behaviour during loading was affected by the heat pulse applied to the core.

(8) To complete the experiments, the samples were hydrostatically loaded to pore collapse failure. This was to determine the stress for onset of yield and check to what degree the stress cycles were performed within the elastic region. The loading rate was the same as that for the stress cycles, i.e. 0.133 MPa/min. The yield stress was defined as the one at which the stress–strain curve deviated from the linear-elastic path for a stress increase greater than 0.25 MPa (Fig. 5). The error was estimated when the deviation from the elastic path reached 1 MPa.

The experimental procedure allows us to compare the strain accumulated during the stress cycles when samples are tested at constant temperature to those subjected to temperature cycle (30 °C–130 °C–30 °C) in between each stress cycle. By using the two different indurated chalks, the mechanical effect of the contact cement is explored, as well as the role of the pore fluid (polar vs. non-polar). Because all the stress cycles were performed at 30 °C, and each cycle started after the previous cycle ended, the effects of temperature on the testing equipment could be excluded, and thus it was assumed that no strain was accumulated between stress cycles. The Biot coefficient was estimated as an average value from cycles 5 to 10 using Eq. (6).

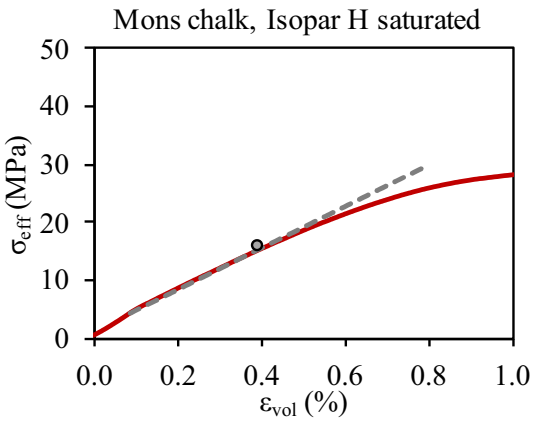

Fig. 5. Yield stress was determined when the stress difference between the measured stress–strain curve and the linear-elastic line exceeded 0.25 MPa.

3. Results

A marked difference was found between samples tested at a constant temperature and those exposed to a temperature cycle between each stress cycle (see Fig. 6), and more strain was accumulated in the samples exposed to temperature variations. The greatest accumulation of irreversible strain was found in the water-saturated Kansas chalk, where the strain accumulated during only a single cycle is approximately equal to the strain accumulated after all ten cycles in a sample tested at constant temperature.

For both chalks and both pore fluids, the samples exposed to temperature cycling have a larger proportion of irreversible strain for each cycle than the samples tested at a constant temperature (Fig. 7). The effect of temperature was pronounced for the water-saturated Kansas chalk samples that had approximately twice the irreversible strain (for each cycle) when the samples were subjected to constant temperature tests. It should be noted that when an additional 11th stress cycle was performed without a prior temperature cycle, the irreversible strain dropped to the value observed in samples tested at constant temperature. This indicates that a temperature pulse of 30 °C–130 °C–30 °C causes the material to behave less elastically.

From the 2nd to the 10th and 11th cycles, the bulk modulus for individual samples did not change significantly, irrespective of constant or cycled temperature tests whereas the samples accumulated plastic strain (Fig. 8 and Table 2). The same behaviour could also be observed for the average loading and unloading slopes (Table 2), in which the stiffness did not change. On average, Kansas chalk had a higher K than Mons chalk, and Kansas chalks saturated with Isopar H oil had a higher stiffness than that saturated by water. For the experiments conducted on Mons chalk, this difference was not observed.

With respect to hydrostatic loading to failure, the Kansas chalk, with a higher degree of contact cementation, is stronger than the Mons chalk (Fig. 9 and Table 3). For hydrostatic failure, pore fluid also plays a role. The samples saturated with water, which is a polar fluid, are weaker than the samples saturated with Isopar H oil (non-polar fluid). We did not observe a significant influence of the temperature cycling on the failure stress.

4. Discussion

All samples tested with temperature cycling accumulated more strain than samples tested at constant temperature during 10 stress cycles (Figs. 6 and 7), even though all stress cycles were performed

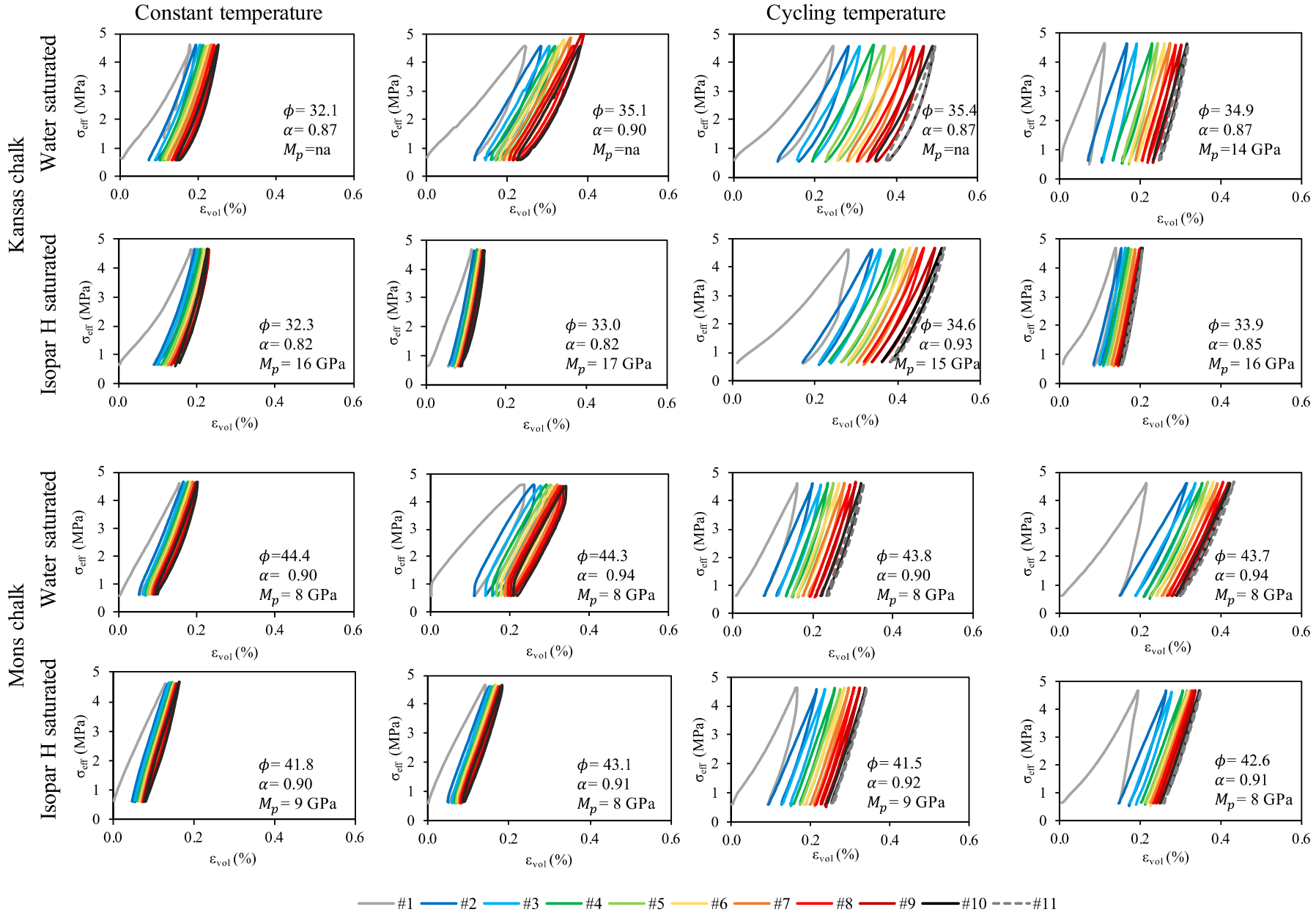

Fig. 6. Stress–strain curves for Kansas (two upper row) and Mons (two lower rows) chalks tested at a constant temperature (10 cycles, the two columns on the left) and with a temperature cycle in between stress cycles (11 cycles, the right two columns).

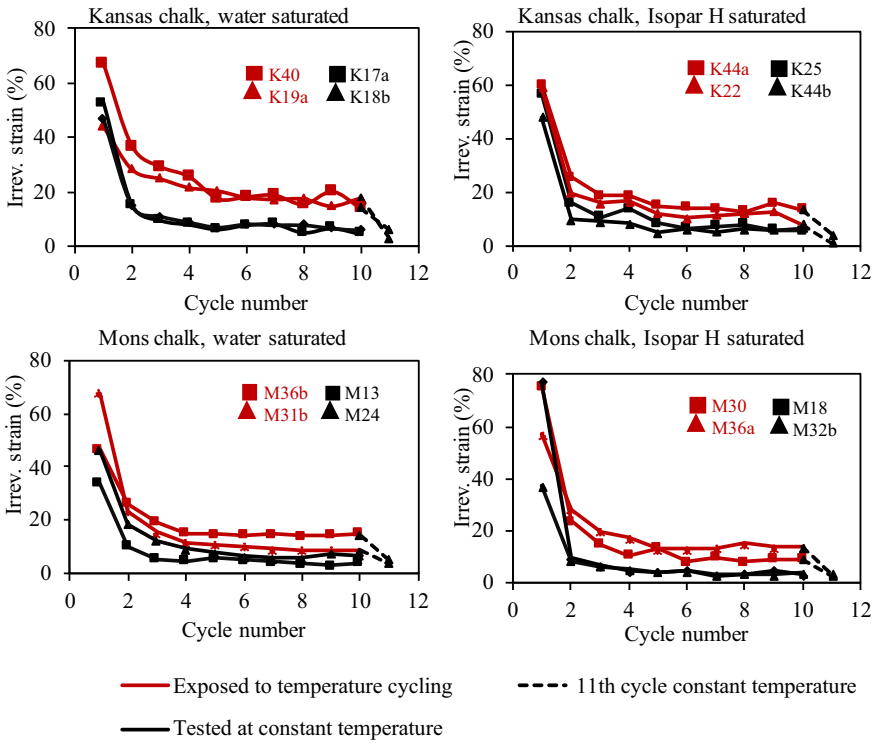

Fig. 7. Irreversible strain for individual stress cycles. The red lines display the test results for samples exposed to temperature cycles, and black lines the samples tested at constant temperature. The dashed line represents the 11th cycle before which the temperature was not varied, in contrast to the 10 cycles before.

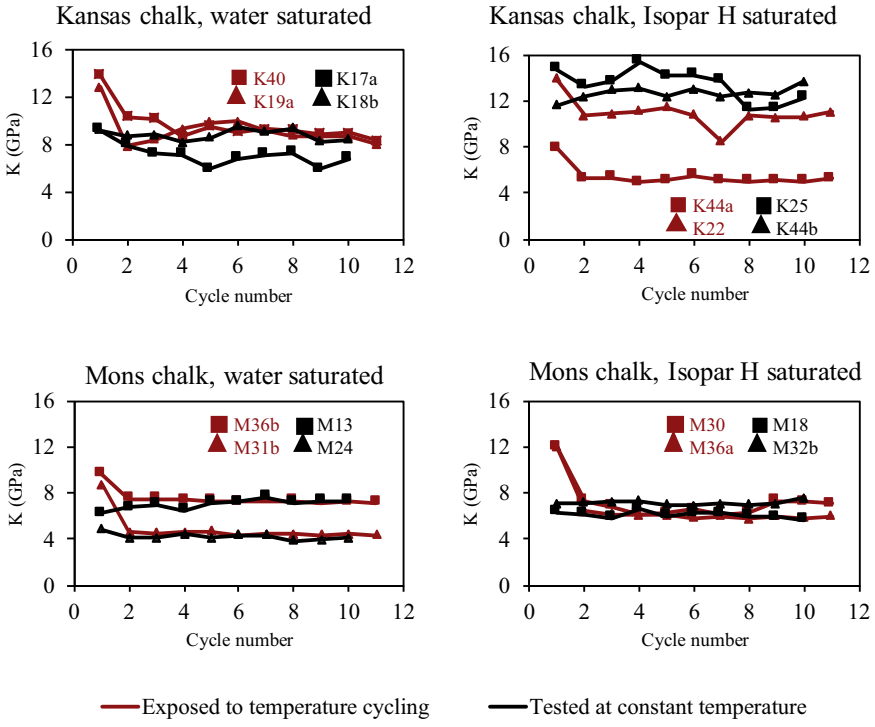

Fig. 8. Elastic bulk modulus *K* from hydrostatic stress cycles (at 30 °C). Red lines represent samples exposed to temperature variation in between each stress cycle, and black lines correspond to samples tested at constant temperature. The high *K* for the first stress cycle, were attributed to equipment alignment or/and closure of microcracks.

Table 2
Average loading and unloading slopes, as well as the elastic bulk modulus through hydrostatic stress cycles.

Sample	Fluid	Temperature cycle	Loading slope (GPa)				Unloading slope (GPa)				Elastic bulk modulus (GPa)			
			1 cycle	3 cycles	7 cycles	10 cycles	1 cycle	3 cycles	7 cycles	10 cycles	1 cycle	3 cycles	7 cycles	10 cycles
K19a	Water	Yes	1.6	2.5	2.7	2.8	2.9	3.5	3.4	3.3	12	8.4	9.2	8.6
K40			3.6	4.7	4.5	4.6	11	6.7	5.7	5.6	13	10.2	9.3	8.9
K17a		No	1.6	2.5	2.5	2.5	3.1	2.6	2.7	2.6	9.2	7.2	7.1	6.8
K18b			2.2	3.5	3.7	3.7	4.7	4.	4.2	4.2	9.2	8.8	9	8.4
K44a	Isopar H oil	Yes	1.4	2.7	2.8	2.7	3.7	3.2	3.1	3.2	7.9	5.3	5.1	5
K22			3	6.3	6.7	7	7.4	7.7	7.4	7.7	14	11	8.9	10.7
K25		No	3.7	6.8	7.1	7.1	6.7	6.9	7	7.1	11.7	13	12.4	13.8
K44b			2.1	3.9	4.1	4.9	3.9	4.1	4.2	5.1	14.8	13.7	13.8	12.3
M36b	Water	Yes	2.6	3.6	3.9	3.9	4.5	4.4	4.5	4.4	9.7	7.5	7.3	7.3
M31b			1.9	2.7	2.9	2.9	6.1	3.1	3.1	3.1	8.8	4.5	4.4	4.4
M13		No	2.5	3.5	3.7	3.6	3.6	3.6	3.7	3.7	6.2	7	7.6	7.3
M24			1.8	1.8	1.8	1.9	3.1	3.5	3.8	3.7	4.8	4.1	4.4	4.1
M30	Isopar H oil	Yes	2.2	3.8	4.1	4.1	8.7	4.5	4.3	4.4	12	6.8	6.1	7.3
M36a			2.4	3.6	4.1	4	7.7	4.5	4.6	4.6	12	6.2	6	5.8
M18		No	2.8	4	4	4	4.6	4.1	4	4	6.3	5.9	6.2	5.7
M32b			3.1	4.6	4.7	4.7	4.9	4.9	4.8	4.9	7.1	7.3	7.1	7.6

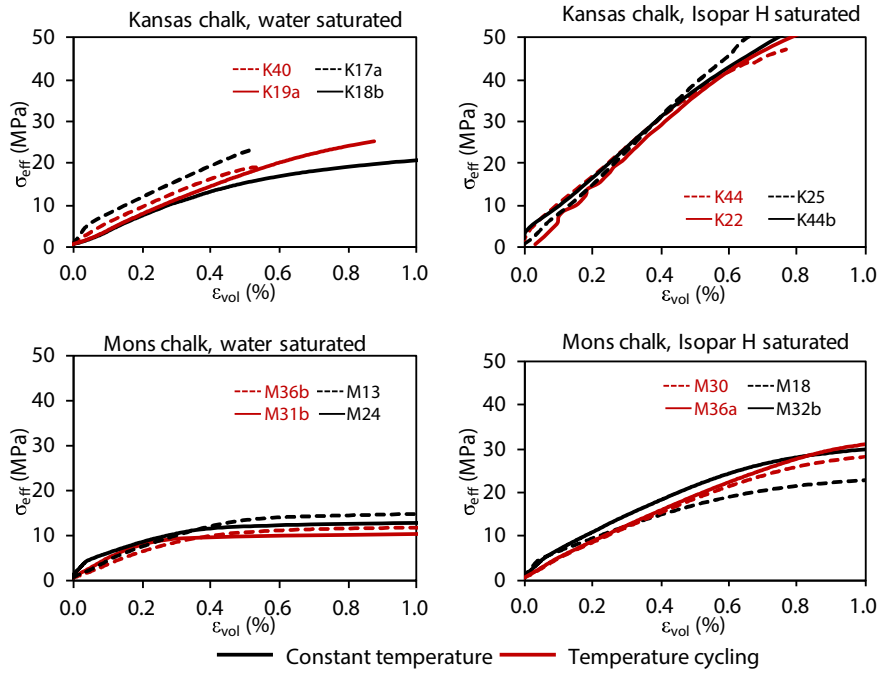

Fig. 9. Hydrostatic failure curves of all the samples tested. Red lines illustrate the test results for samples that have been exposed to temperature cycling, and black lines for the samples tested at a constant temperature.

at 30 °C. The irreversible plastic strain component of the additional 11th stress cycle, which was performed without the temperature cycle in between each stress cycle, dropped to the same value as that of the samples tested at a constant temperature during the whole experiment. This pattern was observed for all tests on both Mons and Kansas chalks saturated with both Isopar H oil and water (Fig. 7). The elastic bulk modulus *K*, however, did not vary significantly from the 2nd to the 10th cycle for either the temperature cycle or the constant temperature tests (Fig. 8), indicating that the elastic behaviour remains the same even though plastic permanent damage accumulates. In Fig. 6, the temperature cycle between each hydrostatic stress cycle leads to greater accumulated strain over the 10th and 11th cycles, and this behaviour is attributed to plasticity effects rather than the changes in elastic behaviour. Furthermore, temperature cycles did not significantly influence the yield strength, and no significant difference after testing could be observed between the samples that had been or not exposed to temperature cycling (Fig. 9). The effect of water weakening, however, was significant, as the hydrostatic yield stress reduced from 13.2–16.3 MPa for Isopar H oil-saturated to 7.9–10.3 MPa for water-saturated Mons chalk, and from 32.2–36.8 MPa to 12.9–18.7 MPa for Kansas chalk (Table 3).

As shown in Fig. 7, the irreversible strain was consistent for the duplicated experiments. However, the total strain accumulated varied for some of the duplicates (Fig. 6). A significant difference between duplicates was found for the Kansas chalk samples saturated with Isopar H oil that had been exposed to temperature cycles between stress cycles. One sample accumulated 0.2% and the other accumulated 0.5% volumetric strain during the tests (Fig. 6). This could be due to the difference in elastic modulus of the two samples. Even though the Kansas chalk samples were cycled at a smaller proportion of yield stress (33% and 40% for water-saturated

Table 3
Yield failure of all samples and comparison to the maximum stress during a hydrostatic cycle. The maximum stress of 5.2 MPa during a hydrostatic cycle is well below the yield failure in all cases.

Sample	Saturating fluid and constant/cycled temperature	Yield failure (MPa)	Percentage of maximum stress (5.2 MPa) to yield stress (%)
K19a	Water/cycle	12.9 ± 2.8	40
K40	Water/cycle	15.9 ± 3.2	33
K17a	Water/constant	18.7 ± 4.4	28
K18b	Water/constant	16.7 ± 4.5	31
K44a	Isopar H oil/cycle	35.2 ± 6.8	15
K22	Isopar H oil/cycle	34.4 ± 4.6	14
K25	Isopar H oil/constant	36.8 ± 6.4	16
K44b	Isopar H oil/constant	32.2 ± 4.7	15
M36b	Water/cycle	8.5 ± 1.9	62
M31b	Water/cycle	7.9 ± 2.2	66
M13	Water/constant	10.3 ± 2.6	51
M24	Water/constant	9.7 ± 2	53
M30	Isopar H oil/cycle	15.2 ± 5.7	34
M36a	Isopar H oil/cycle	16.3 ± 5.4	32
M18	Isopar H oil/constant	13.2 ± 4	39
M32b	Isopar H oil/constant	15.5 ± 5.3	33

chalks, and 14% and 16% for oil-saturated chalks, see Table 3 and Fig. 6), it showed that the temperature cycling led to more or equal amounts of volumetric strain after 11 cycles than the cycling performed on Mons chalk where the peak cycle stress was 62% and 66% of yield stress for the water-saturated samples and 32% and 34% for oil-saturated samples. It would be expected that when approaching the failure envelope, more plastic damage would accumulate, but this was not observed.

In order to find how the accumulated strain is linked to other measurable parameters, the total accumulated strain from the 2nd to the 10th cycle (ε_{tot}) was plotted against the initial porosity (ϕ) and the Biot coefficient (α) (Fig. 10). The first cycle was omitted from these correlations to avoid inherent large variability observed in the first load cycle (Fig. 6) as seen for all the tests. Even though the statistical significance is limited, it may be seen that the Kansas-Isopar H experiments accumulate more strain (open green circles) when both the porosity and Biot coefficient increase (Fig. 10a and c). Furthermore, the experiments on water-saturated Kansas chalk displayed a positive correlation between ε_{tot} and ϕ (closed green circles), while ε_{tot} was not correlated to the Biot coefficient (Fig. 10a and c). For Mons chalk samples, the same correlations were not observed, neither between ε_{tot} and ϕ, nor between ε_{tot} and α. As such, a univocal statistical pattern relating the porosity and Biot coefficient to the total accumulated strain for both Kansas and Mons chalks cannot be observed. It is interesting to note that, however, the highly indurated chalk displays such a correlation, whilst the less indurated Mons chalk does not.

Fig. 10b and d displays the correlations of ε_{tot} vs. ϕ and ε_{tot} vs. α, respectively, discriminated by testing methods. Here the samples are split into four groups in combination with Kansas chalk (circles) and Mons chalk (triangles), and constant temperature (black) and temperature cycles (red). For all four groups, positive correlations between volumetric strain and porosity (Fig. 10b), and between ε_{tot} and α can be seen. This observation is interesting because more.

For each individual stress cycle, approximately double irreversible strain was accumulated if the temperature cycling was performed, as opposed to the experiments at a constant temperature. This plastic component was most pronounced for the water-

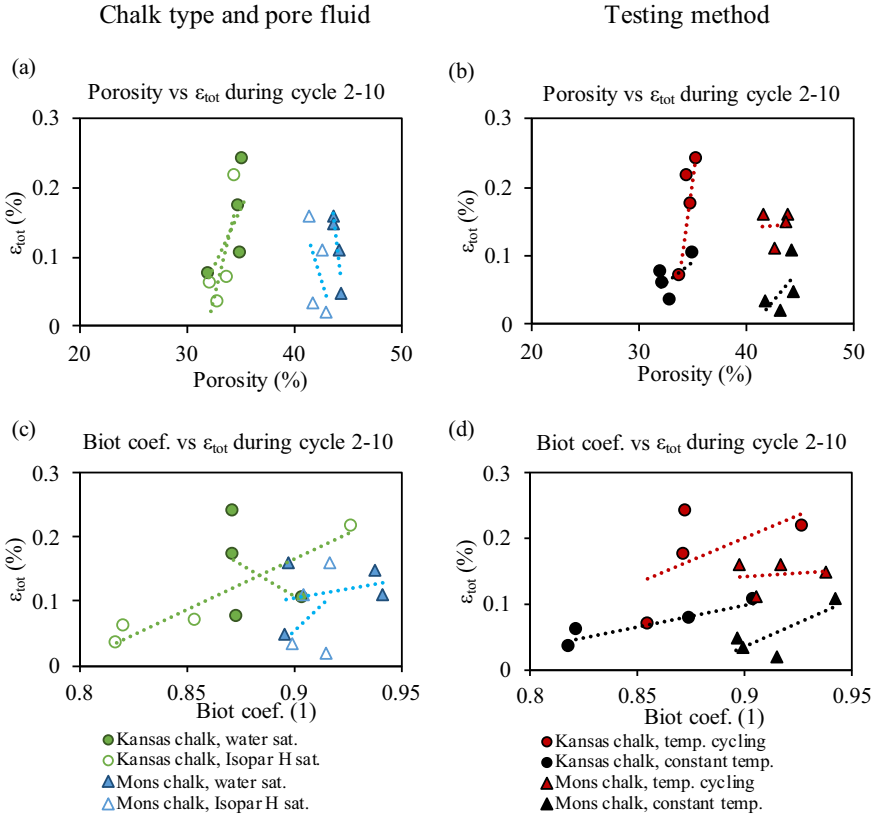

Fig. 10. Correlation between the total strain accumulated between cycles 2–10 and saturation porosity (top) and Biot coefficient (bottom). On the left, the correlation is made for different chalk types and their saturating fluids. No uniform trend was found. On the right, the correlation is made according to the testing method, whether the chalk samples were exposed to a constant temperature or to temperature cycling. These correlations all display a similar trend, indicating that the total strain accumulated increases with the increasing porosity and Biot coefficient.

saturated and highly indurated Kansas chalk samples (Fig. 7). The two chalk types behaved differently when saturated with water, but no significant behavioural difference was observed in Isopar H oil-saturated samples. The highly indurated Kansas chalk accumulated both more total strain and more irreversible strain within each stress cycle than Mons chalk when saturated with water. This indicates that the greater amount of contact cementation (lower Biot coefficient) is more susceptible to anisotropic thermal expansion and contraction of calcite particles when saturated with water, a polar fluid.

The saturating fluid thus plays an important role in mechanical testing. Our data show that water saturation reduces hydrostatic yield strength (Fig. 9). This is in line with the conclusions of other works (Madland et al., 2002; Risnes et al., 2005). Water is a polar fluid and it can be adsorbed to the calcite surfaces in chalk. Isopar H oil is no-polar fluid and cannot be adsorbed to the calcite surface.

Calcite crystals have surfaces populated by positively charged Ca^{2+} and negatively charged CO_3^{2-} surface sites (Stipp et al., 1999). At the basic equilibrium-pH of water and calcite, adsorption of divalent positive ions (Ca^{2+}) and monovalent negative ions (HCO_3^-) causes an overall positive surface charge. Røyne et al. (2011) used glycol-water mixtures to measure surface energy of calcite depending on water concentration, and they found that the surface energy decreased with increasing water concentration. The decline in hydrostatic yield strength by saturation could be related to the observations of fracture generation in dry calcite. The energy needed to create a calcite surface depends on the presence of water, where the energy needed for generating a dry surface is 0.32 J/m^2, whereas it is 0.15 J/m^2 for a fully hydrated calcite surface (Røyne et al., 2011). This means that it takes almost double the energy to create a dry calcite surface than that for a hydrated one, and hence in water-saturated samples, it would be easier to break contact cementation and make a new surface between two neighbouring particles. When employing these results to the fracture formation between calcite particles placed next to each other with a non-zero difference in c-axis angle, thermally induced strain would result in thermal stress concentrations within the contact cement, which would lead to bond breakage when the energy for generating a new surface is minimised.

When the saturating fluid has electrical charge exchange with the calcite surface, it creates an electrical double layer (Al Mahrouqi et al., 2017). If we assume that the thickness of the charged layer is directly proportional to the Debye length, then the thickness of the layer also depends on the temperature, and it increases with increasing temperature. Increasing this area of repulsion between particles would stress the areas of contact cementation extremely, and thus more indurated samples would be more influenced at higher temperatures. However, as it was not observed that yield stress depends on whether the sample has been exposed to temperature cycling or not, but a greater plastic strain accumulation was observed at cycled temperature, it is proposed that increasing the length of the electrical double layer enhances the number of contacts with broken cement (micro-fractures). This would not affect the overall strength, which depends on the strength of the weakest bond rather than the number of weak bonds.

Experimental results imply that contact cementation breakage affects neither yield strength nor bulk modulus, but rather directly the amount of irreversible strain. The temperature sensitivity occurs to a lower extent for the less cemented Mons chalk, because cementation is not contributing as much to Mons chalk stiffness and strength, as it does for Kansas chalk, which gains its higher stiffness and strength from higher degree of contact cementation.

Even for elastic-perfectly metallic electric alloys, such as the compound of lead and tin (Pb/Sn) used in microelectronic packaging, it demonstrates that inelastic strain accumulates during 100 temperature cycles between 0 °C and 75 °C. This accumulation was found to be caused by the component bonded to the alloy having a different thermal expansion coefficient from the alloy itself (Dishongh et al., 2002). As such, stress concentrations induced by the differences in thermal strain at given material contacts lead to failure – a microscopic effect that may propagate to the mesoscopic scale. As such, due to the anisotropic thermal expansion of calcite, chalk samples with higher area of contact cementation are expected to be more influenced by temperature variation.

5. Conclusions

This paper aimed to better understand the mechanical stability of chalk during water injection, which can cause temperature to fluctuate. In response to temperature fluctuation, the anisotropic thermal expansion of calcite crystals induces thermal stress that results in accumulation of irreversible strain. From the experiments performed in this study, all samples exposed to temperature cycling accumulated more strain than the samples tested at a constant temperature. This was specifically pronounced for water-saturated Kansas chalk, which has a relatively high induration and a high degree of contact cementation. Polarity of the saturating fluid plays a greater role in more indurated chalk exposed to temperature cycling. However, temperature cycling had an effect on irreversible strain accumulated, but no significant influence on elastic modulus or yield stress. Furthermore, it was also found that the peak in each stress cycle relative to the failure strength is not the deterministic parameter for the permanent damage accumulated during stress and temperature cycles. This is conclusive that temperature cycling resulted in an increase in the number of micro-fractures, which hence accumulated more strain during stress variation in the elastic domain, but did not influence the overall strength of the samples. Our results indicate that the risk of degrading the mechanical integrity of chalk by temperature variation is more relevant for deeper and thus more contact-cemented chalk reservoirs, with low Biot coefficient, than for shallower chalk reservoirs with high Biot coefficient.

Conflicts of interest

The authors wish to confirm that there are no known conflicts of interest associated with this publication and there has been no significant financial support for this work that could have influenced its outcome.

Acknowledgments

The authors acknowledge the Research Council of Norway and the industry partners, ConocoPhillips Skandinavia AS, Aker BP ASA, Eni Norge AS, Total E&P Norge AS, Equinor ASA, Neptune Energy Norge AS, Lundin Norway AS, Halliburton AS, Schlumberger Norge AS, Wintershall Norge AS, and DEA Norge AS, of the National IOR Centre of Norway for support. Espen Jettestuen is thanked for constructive discussion.

References

Al Mahrouqi D, Vinogradov J, Jackson MD. Zeta potential of artificial and natural calcite in aqueous solution. Advances in Colloid and Interface Science 2017;240:60–76.
Baud P, Zhu WL, Wong TF. Failure mode and weakening effect of water on sandstone. Journal of Geophysical Research: Solid Earth 2000;105(B7):16371–89.
Becattini V, Motmans T, Zappone A, Madonna C, Haselbacher A, Steinfeld A. Experimental investigation of the thermal and mechanical stability of rocks for high-temperature thermal-energy storage. Applied Energy 2017;203:373–89.
Chen LJ, He J, Chao JQ, Qin BD. Swelling and breaking characteristics of limestone under high temperatures. Mining Science and Technology (China) 2009;19(4):503–7.

Collins BD, Stock GM, Eppes MC, Lewis SW, Corbett SC, Smith JB. Thermal influences on spontaneous rock dome exfoliation. Nature Communications 2018;9:762. https://doi.org/10.1038/s41467-017-02728-1.

De Andrade J, Sangesland S, Todorovic J, Vrålstad T. Cement sheath integrity during thermal cycling: a novel approach for experimental tests of cement systems. In: SPE bergen one day seminar. Society of Petroleum Engineers (SPE); 2015. https://doi.org/10.2118/173871-MS.

Dishongh T, Basaran C, Cartwright AN, Zhao Y, Liu H. Impact of temperature cycle profile on fatigue life of solder joints. IEEE Transactions on Advanced Packaging 2002;25(3):433–8.

Fabricius IL. Burial stress and elastic strain of carbonate rocks. Geophysical Prospecting 2014;62(6):1327–36.

Hansen KK, Leksø H, Grelk B. Assessment of the durability of marble cladding by laboratory exposure compared to natural exposure. In: Carmeliet J, Hens H, Vermeir G, editors. Research in building physics: proceedings of the 2nd international conference on building physics. CRC Press; 2003. p. 267–71.

Henriksen AD, Fabricius IL, Borre MK, Korsbech U, Theilgaard AT, Zandbergen JB. Core density scanning, degree of induration and dynamic elastic moduli of Palaeogene limestone in the Copenhagen area. Quarterly Journal of Engineering Geology and Hydrogeology 1999;32(2):107–17.

Hermansen H, Thomas LK, Sylte JE, Aasboe BT. Twenty five years of Ekofisk reservoir management. In: SPE annual technical conference and exhibition. Society of Petroleum Engineers (SPE); 1997. https://doi.org/10.2118/38927-MS.

Hua W, Dong SM, Li YF, Xu JG, Wang QY. The influence of cyclic wetting and drying on the fracture toughness of sandstone. International Journal of Rock Mechanics and Mining Sciences 2015;78:331–5.

Katika K, Addassi M, Alam MM, Fabricius IL. The effect of divalent ions on the elasticity and pore collapse of chalk evaluated from compressional wave velocity and low-field nuclear magnetic resonance (NMR). Journal of Petroleum Science and Engineering 2015;136:88–99.

Lebedev M, Wilson MEJ, Mikhaltsevitch V. An experimental study of solid matrix weakening in water-saturated Savonnieres limestone. Geophysical Prospecting 2014;62(6):1253–65.

Lisabeth HP, Zhu WL. Effect of temperature and pore fluid on the strength of porous limestone. Journal of Geophysical Research: Solid Earth 2015;120(9):6191–208.

Madland MV, Korsnes RI, Risnes R. Temperature effects in Brazilian, uniaxial and triaxial compressive tests with high porosity chalk. In: SPE annual technical conference and exhibition. SPE; 2002. https://doi.org/10.2118/77761-MS.

Mavko G, Mukerji T, Dvorkin J. The rock physics handbook: tools for seismic analysis in porous media. Cambridge, UK: Cambridge University Press; 1998.

Megawati M, Hiorth A, Madland MV. The impact of surface charge on the mechanical behavior of high-porosity chalk. Rock Mechanics and Rock Engineering 2013;46(5):1073–90.

Okeson MA, Kellogg KG, Kallmeyer AR. Impact damage growth in fiberglass/epoxy laminates subjected to moisture and low temperature thermal cycling. In: Ayer R, Chung JS, Ames N, Wheat HG, editors. Proceedings of the 16th international offshore and polar engineering conference. International Society of Offshore and Polar Engineers (ISOPE); 2006. p. 279–86.

Olsen C, Christensen HF, Fabricius IL. Static and dynamic Young's moduli of chalk from the North Sea. Geophysics 2008;73(2):E41–50.

Ravnås C. Petrophysical and rock mechanical properties of heat treated chalk. Kongens Lyngby: Technical University of Denmark; 2017.

Risnes R, Madland MV, Hole M, Kwabiah NK. Water weakening of chalk – mechanical effects of water-glycol mixtures. Journal of Petroleum Science and Engineering 2005;48(1–2):21–36.

Rosenholtz JL, Smith DZ. Linear thermal expansion of calcite, var. Iceland spar, and Yule marble. American Mineralogist 1949;34(11–12):846–54.

Røyne A, Bisschop J, Dysthe DK. Experimental investigation of surface energy and subcritical crack growth in calcite. Journal of Geophysical Research: Solid Earth 2011;116(B4). https://doi.org/10.1029/2010JB008033.

Stipp S, Brady PV, Ragnarsdottir KV, Charlet L. Geochemistry in aqueous systems – a special issue in honor of Werner Stumm – preface. Geochimica et Cosmochimica Acta 1999;63(7):3121–31.

Wasantha PLP, Ranjith PG. Water-weakening behavior of Hawkesbury sandstone in brittle regime. Engineering Geology 2014;178:91–101.

Weiss T, Siegesmund S, Fuller ER. Thermal degradation of marble: indications from finite-element modelling. Building and Environment 2003;38(9–10):1251–60.

Yang YC, Zhou JW, Xu FG, Xing HG. An experimental study on the water-induced strength reduction in Zigong argillaceous siltstone with different degree of weathering. Advances in Materials Science and Engineering 2016. https://doi.org/10.1155/2016/4956986.

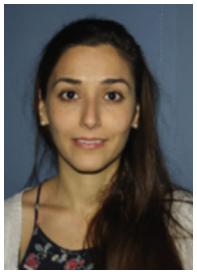

T. Voake is currently pursuing her PhD degree in Petroleum Technology at the University of Stavanger, Norway. She obtained her MSc degree in Geophysics from Memorial University of Newfoundland, and Honours Bachelor of Science (HBSc) degree from the University of Toronto, Canada. She has worked on numerous field and laboratory projects classifying rock physical properties. She has previously worked in the petroleum industry for a software development company.